RSC Mechanochemistry

ROYAL SOCIETY OF CHEMISTRY

PAPER

View Article Online
View Journal | View Issue

Cite this: *RSC Mechanochem.*, 2025, **2**, 603

Thermodynamic and kinetic study of the effect of LiCl and NaCl on the thermal dehydrogenation of $Ca(AlH_4)_2$†

Franziska Habermann,[a] Anneliese Wirth,[a] Konrad Burkmann,[a] Jakob Kraus,[b] Bianca Störr,[a] Hartmut Stöcker,[cd] Jürgen Seidel,[a] Jens Kortus,[b] Roman Gumeniuk,[c] Klaus Bohmhammel[a] and Florian Mertens *[a]

Received 3rd December 2024
Accepted 12th May 2025

DOI: 10.1039/d4mr00140k

rsc.li/RSCMechanochem

The presented work sets out to investigate the dehydrogenation behaviour of $Ca(AlH_4)_2$ + 2MCl (M = Li, Na) mixtures. In contrast to the by-product NaCl, which does not affect the decomposition of $Ca(AlH_4)_2$, LiCl influences its dehydrogenation onward from the formation of $CaAlH_5$. Thermodynamic calculations were used to support and explain these findings as well as to investigate the potential of $Ca(AlH_4)_2$ and $CaAlH_5$ for reversible hydrogen storage applications. For this purpose, their heat capacity functions and absolute entropies were determined in this study.

1 Introduction

In the context of the transition to a renewable energy-based economy, alloys, metal hydrides or complex hydrides are widely discussed regarding their suitability for solid-state hydrogen storage applications.[1–11] In this context, light metal complex hydrides have been intensively studied since Bogdanovic and Schwickwardi reported reversible hydrogen storage in Ti-doped $NaAlH_4$.[12] However, these investigations were mainly focused on the alkaline metal alanates $LiAlH_4$ and $NaAlH_4$, leaving the alanates of the earth alkaline metals less studied.

$Ca(AlH_4)_2$ was first synthesised by Finholt *et al.* in 1955.[13] The alanate was prepared in dimethyl ether starting from AlX_3 (X = Cl, Br) and CaH_2. Since the mechanochemical synthesis route was established for complex hydrides, $Ca(AlH_4)_2$ was also produced mechanochemically *via* metathesis reactions between $MAlH_4$ (M = Li, Na) and $CaCl_2$.[14–16]

The thermal dehydrogenation of $Ca(AlH_4)_2$ proceeds *via* four steps. First, the alanate decomposes to $CaAlH_5$ and Al (reaction (1)). In the second step $CaAlH_5$ dehydrogenates to CaH_2 and Al (reaction (2)). The formed CaH_2 decomposes in the following accompanied by the formation of $CaAl_4$ in the third (reaction (3)) and $CaAl_2$ (reaction (4)) in the fourth step. Besides the first step, which occurs exothermically, all other reactions are endothermic.[16–18]

$$Ca(AlH_4)_2 \rightarrow CaAlH_5 + Al + \frac{3}{2}H_2 \quad (1)$$

$$CaAlH_5 \rightarrow CaH_2 + Al + \frac{3}{2}H_2 \quad (2)$$

$$xCaH_2 + 4xAl \rightarrow xCaAl_4 + xH_2 \quad (3)$$

$$(1-x)CaH_2 + xCaAl_4 + (2-4x)Al \rightarrow CaAl_2 + (1-x)H_2 \quad (4)$$

Recently, we disproved the common assumption that the by-products of the mechanochemical synthesis of complex hydrides behave inertly by showing that the pathway of the thermal dehydrogenation of $Sr(AlH_4)_2$ depends on them.[10] In this study, the influence of LiCl and NaCl on the decomposition route and dehydrogenation kinetics of $Ca(AlH_4)_2$ was investigated. Thermodynamic computations were employed to support and explain our findings as well as to assess the potential of the complex hydrides for reversible hydrogen storage applications. For that purpose and to complete their thermodynamic characterisation, the heat capacity functions and absolute entropies of $Ca(AlH_4)_2$ and $CaAlH_5$ were determined by means of calorimetry and DFT calculations.

2 Experimental

2.1 Materials

All reactions as well as the handling and storage of the samples were performed under dry argon atmosphere using Schlenk line technique or a MBraun glove box (H_2O and O_2 < 0.1 ppm).

[a]*Institut für Physikalische Chemie, TU Bergakademie Freiberg, Lessingstraße 45, 09599 Freiberg, Germany. E-mail: florian.mertens@chemie.tu-freiberg.de; Tel: +493731393737*

[b]*Institut für Theoretische Pysik, TU Bergakademie Freiberg, Leipziger Straße 23, 09599 Freiberg, Germany*

[c]*Institut für Experimentelle Pysik, TU Bergakademie Freiberg, Leipziger Straße 23, 09599 Freiberg, Germany*

[d]*Center for Efficient High Temperature Processes and Materials Conversion, TU Bergakademie Freiberg, Winklerstraße 5, 09599 Freiberg, Germany*

† Electronic supplementary information (ESI) available. See DOI: https://doi.org/10.1039/d4mr00140k

Argon was obtained from Nippon Gases specified as 99.999% pure. Sodium aluminium hydride ($NaAlH_4$, Sigma Aldrich, 90%, technical grade) and Copper foil (Cu, Puratronic, 99.999%) were used without further purification. Calcium chloride ($CaCl_2$, Alfa Aesar, >96.0%, anhydrous) was dried before use at 150 °C under an argon purge gas flow in a self-built horizontal tube furnace for 24 h. Lithium aluminium hydride ($LiAlH_4$, abcr, 97%) was purified by first dissolving it in diethyl ether and then filtering off the impurities. Subsequently, the solvent was distilled off in vacuum. The residue was dried in vacuum at 55 °C for 12 h. The used diethyl ether ($C_4H_{10}O$, Honeywell Riedel-de-Haen, 99.8%, p.a.) was dried in a MB SPS-800 drying plant.

2.2 Synthetic procedures

2.2.1 Synthesis of $Ca(AlH_4)_2$ + 2MCl (M = Li, Na). $Ca(AlH_4)_2$ + 2MCl was prepared mechanochemically starting from $CaCl_2$ and $MAlH_4$. The milling of the reactants, which were used in the stoichiometric ratio 1 : 2, was performed by means of a Fritsch Pulverisette 6. The milling vial (12 mL) and balls (each 7 g) were made of tungsten carbide. Three balls were used, resulting in a bpr of *ca.* 40. A milling cycle consisted of 15 min of milling at 500 rpm and a pause of 5 min. For the synthesis of $Ca(AlH_4)_2$ + 2NaCl 32 cycles were run adding up to a total milling time of 8 h. Only 12 cycles (3 h of milling) were necessary for the complete conversion of $CaCl_2$ and $LiAlH_4$.

2.2.2 Identification of the products of the thermal dehydrogenation of $Ca(AlH_4)_2$. The samples were heated to the respective decomposition temperature by means of a self-built horizontal tube furnace. After weighing in 50–190 mg of $Ca(AlH_4)_2$ + 2MCl (M = Li, Na) under an inert atmosphere, the mixtures were put in a corundum crucible which was then placed within a quartz tube, which enabled an inert handling of the samples. The mixtures were heated in a stream of argon at a heating rate of 5 K min^{-1} to 290 °C and 400 °C in the case of $Ca(AlH_4)_2$ + 2NaCl. $Ca(AlH_4)_2$ + 2LiCl was heated to 260 °C, 290 °C, and 440 °C under the same conditions. The samples were cooled down to room temperature without active cooling.

The phase composition of the cooled down samples was analysed using X-ray diffraction.

2.3 Characterisation techniques

2.3.1 X-ray diffraction. The characterisation of the samples by means of X-ray diffraction was performed using a Bruker D2 Phaser X-ray diffractometer (Cu Kα radiation) equipped with a Lynxeye® detector. The X-ray powder patterns were collected with a step size of 0.05° and a dwell time of 1 s. The X-ray tube was operated at 30 kV and 10 mA. The sample holder was covered with a polyethylene foil in order to protect the sample from oxygen and moisture.

Reference diffractograms from the ICSD[19] were used to identify the present phases.

2.3.2 *In situ* X-ray diffraction. *In situ* X-ray diffraction between room temperature and 270 °C was performed using a Bruker D8 Advance X-ray diffractometer equipped with an Anton Paar HTK 1200N oven chamber with capillary attachment. The instrument consisted of a molybdenum X-ray tube operated at 50 kV and 40 mA with focusing Göbel mirror and a Dectris Eiger2R 500K detector. Axial and radial Soller collimators were installed to improve peak shape and suppress air scattering. The samples were prepared in quartz glass capillaries of 0.5 mm diameter that were filled under argon and sealed against air. The measurements were performed with a 2Θ step size of 0.02° and a dwell time of 1 s per step.

2.3.3 TG-DSC-FTIR. A Sensys TG-DSC (Setaram) was employed to carry out TG-DSC-FTIR measurements. About 10 mg of the samples were weighed in under an inert atmosphere and placed in a corundum crucible. Measurements were performed up to 450 °C at heating rates of 2 K min^{-1}, 5 K min^{-1}, 8 K min^{-1}, and 10 K min^{-1} under an argon purge gas flow of 20 mL min^{-1}. A H_2-sensor (thermal conductivity sensor AGM22, SENSORS) and FTIR (Varian 3100 FT-IR, Excalibur Series) were used to identify the gaseous decomposition products at the purge gas outlet.

2.3.4 Heat capacity measurements. Heat capacity measurements from 2 K to 298 K were performed on the Physical Property Measurement System (PPMS) DynaCool-12 (Quantum Design) using its heat capacity function.[20] The samples were encased in copper foil because the device does not allow an inert sample placement. For that purpose, 21.6 mg of $Ca(AlH_4)_2$ + 2LiCl were weighed in, placed within a self-built copper crucible[21] and then pressed to form a pellet. All these operations were carried out under an inert atmosphere.

To ensure a good thermal contact between the sample and the sample platform during the measurement, Apiezon N grease was applied. The heat capacity of the encased sample was automatically calculated by the PPMS software Multivu by subtracting the addenda measurements (sample platform and grease) from that of the encased sample (encased sample, sample platform, and grease).[22] Using eqn (5) and literature data for copper,[23] the heat capacity of the sample was obtained from that of the encased one.

$$C_p^{\text{encased sample}} = x^{\text{sample}} C_p^{\text{sample}} + x^{\text{Cu}} C_p^{\text{Cu}} \quad (5)$$

A DSC 111 (Setaram) was used to carry out heat capacity measurements in the temperature range from 283 K to 360 K. These measurements were performed using a C_p-by-step technique as described in ref. 20. After weighing the samples in under inert atmosphere (144.9 mg $Ca(AlH_4)_2$ + 2NaCl and 153.8 mg $Ca(AlH_4)_2$ + 2LiCl) they were placed in an aluminium crucible which was then sealed with an aluminium cap. The applied temperature programme consisted of four temperature steps (6 K, 3 K min^{-1}) in the temperature range between 303 K and 363 K and six temperature steps (10 K, 3 K min^{-1}) between 303 K and 363 K. Before and after each temperature step, the temperature was kept constant for one hour. The same method was applied to the sample, the reference (sapphire), and the blank (empty capped aluminium crucible).

The heat capacity of the sample (c_p) at the mean temperature of the step was derived using eqn (6). The start and end time of the respective heat flow peak ($\dot{q}$) are denoted by t_i and t_{i+1} and the masses of the reference and sample are given by m_{ref} and m_{sam}. The symbol $c_{p,ref}$ represents the heat capacity of the reference material at the mean temperature of the step. The corresponding data were taken from ref. 24.

$$c_p = \frac{\int_{t_i}^{t_{i+1}} \dot{q}_{sam}\,dt - \int_{t_i}^{t_{i+1}} \dot{q}_{blank}\,dt}{\int_{t_i}^{t_{i+1}} \dot{q}_{ref}\,dt - \int_{t_i}^{t_{i+1}} \dot{q}_{blank}\,dt} \cdot \frac{m_{ref}}{m_{sam}} \cdot c_{p,ref} \quad (6)$$

2.4 Calculations using density functional theory (DFT)

Density functional theory (DFT[25,26]) computations were performed to complement the experimental characterisation techniques. All computations were conducted using the plane-wave Quantum ESPRESSO program,[27–29] version 6.7, in combination with PAW pseudopotentials[30] obtained from version 1.0.0 of the PSlibrary.[31] The generalised-gradient exchange–correlation functional by Perdew, Burke, and Ernzerhof (PBE[32]) was applied in all cases.

3 Results & discussion

3.1 Synthesis of $Ca(AlH_4)_2$ + 2MCl (M = Li, Na)

$Ca(AlH_4)_2$ + 2MCl samples were synthesised converting $CaCl_2$ and $MAlH_4$ (reactions (7) and (8)). Both samples were characterised using X-ray diffraction. Since only reflections belonging to the expected products ($Ca(AlH_4)_2$ and MCl) can be observed in the measured diffractograms (Fig. 1), we deem both syntheses successful.

$$CaCl_2 + 2LiAlH_4 \rightarrow Ca(AlH_4)_2 + 2LiCl \quad (7)$$

$$CaCl_2 + 2NaAlH_4 \rightarrow Ca(AlH_4)_2 + 2NaCl \quad (8)$$

3.2 Thermal dehydrogenation of $Ca(AlH_4)_2$ + 2MX (M = Li, Na)

The influence of LiCl and NaCl on the thermal decomposition behaviour of $Ca(AlH_4)_2$ was investigated by means of TG-DSC (Fig. 2). It has to be noted that the weight losses were normalised to $Ca(AlH_4)_2$ in order to enable a comparison of both mixtures. The theoretical weight losses according to the proceeding of reactions (1)–(4) are indicated by dashed horizontal lines. Since the value of x is unknown, only the weight loss corresponding to both eqn (3) and (4) is depicted.

The total weight loss of both mixtures is smaller than the theoretical one, indicating a minor decomposition of the alanate during the milling procedure.

The proceeding of the thermal dehydrogenation of the $Ca(AlH_4)_2$ + 2NaCl mixture agrees with the literature reports.[16–18,33] According to both the TG and DSC measurement, the decomposition takes place in four separate steps. As expected, each step is accompanied by a release of hydrogen.

The unknown variable x in the decomposition reactions (3) and (4) was determined to be 0.5 from the ratio of the weight losses associated with the third and fourth step.

The only point where the results differ from the literature reports is the DSC effect belonging to the first dehydrogenation event. Contrary to the literature,[16–18] where eqn (1) occurs exothermically, we observe a DSC effect consisting of both an endothermic and an exothermic signal. This behaviour becomes more pronounced at higher heating rates as can be seen in Fig. 6. In recent studies on $Mg(AlH_4)_2$ (ref. 9) and $Sr(AlH_4)_2$ (ref. 10) we found the DSC events corresponding to their decomposition to be composed of an endo- and exothermic peak as well.

This behaviour indicates two overlapping reactions. Since $Ca(AlH_4)_2$ and $Sr(AlH_4)_2$ dehydrogenate similarly,[34] we propose reactions (9) and (10) based on those suggested for $Sr(AlH_4)_2$ in ref. 10. Then, the endothermic signal would result from the dehydrogenation of $Ca(AlH_4)_2$ to CaH_2 and AlH_3 and the exothermic one from the consecutive formation of $CaAlH_5$.

$$Ca(AlH_4)_2 \rightarrow CaH_2 + AlH_3 + Al + \frac{3}{2}H_2 \quad (9)$$

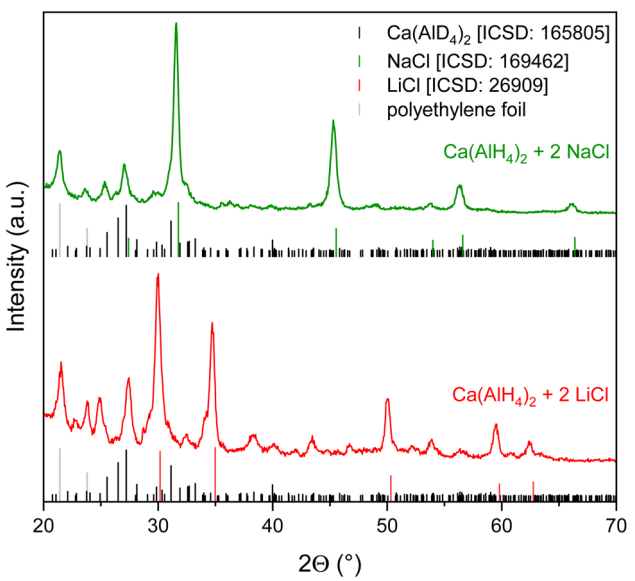

Fig. 1 X-ray powder diffraction patterns of $Ca(AlH_4)_2$ + 2MCl (M = Li, Na).

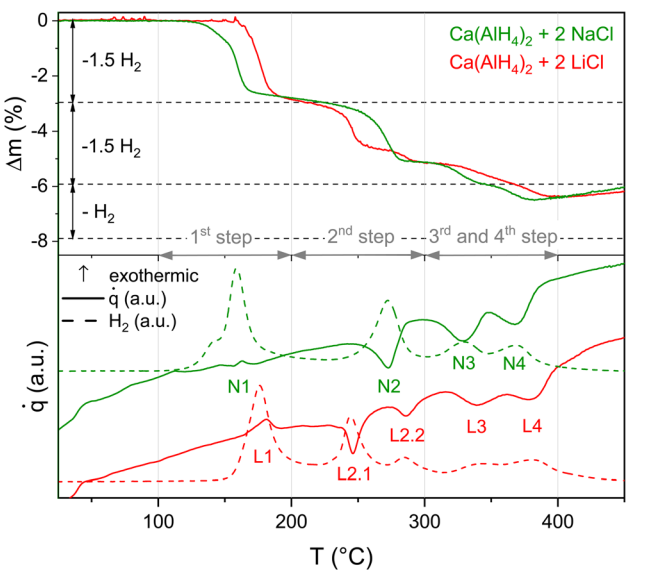

Fig. 2 TG-DSC measurements of $Ca(AlH_4)_2$ + 2MCl (M = Li, Na), heating rate 5 K min^{-1}, H_2 traces are given in a.u.

$$CaH_2 + AlH_3 \rightarrow CaAlH_5 \quad (10)$$

While no significant differences between the decomposition of $Ca(AlH_4)_2$ + 2NaCl and $Ca(AlH_4)_2$ + 2LiCl are apparent in the first dehydrogenation step, the following decomposition behaviour seems to depend on the halide. Hence, the by-product does not influence the decomposition of $Ca(AlH_4)_2$ itself but that of $CaAlH_5$.

The difference in the dehydrogenation behaviour becomes especially apparent in the second decomposition step. In contrast to the NaCl sample, which dehydrogenates in one step, the LiCl mixture decomposes in two sub-steps. Both sub-steps correlate with a hydrogen release. Moreover, the effects associated with the third and fourth step overlap in case of $Ca(AlH_4)_2$ + 2LiCl.

Furthermore, the comparison of the onset temperatures of the decomposition reactions (Table 1) shows that the first dehydrogenation event occurs at higher temperatures for the LiCl mixture than for the NaCl one. This difference is probably due to the different milling periods, which result in different particle sizes and thus different decomposition kinetics. Since the NaCl mixture was milled longer, its $Ca(AlH_4)_2$ probably dehydrogenates at lower temperatures.

In contrast to the first step, the opposite trend can be observed for the onset temperatures of the second step. Therefore, it seems unlikely that this behaviour is due to different decomposition kinetics. Instead, the proceeding reaction probably changes depending on the by-product.

In order to further investigate the effect of the by-product on the dehydrogenation behaviour, the corresponding decomposition products were identified by means of X-ray diffraction. Since the quality of the X-ray diffraction patterns of the samples after the TG-DSC measurements was poor, samples similar to those had to be synthesised *ex situ*. For this purpose, the $Ca(AlH_4)_2$ + 2MCl mixtures were heated to the respective temperature of interest with a heating rate of 5 K min^{-1} in a self-built horizontal tube furnace. The X-ray diffraction patterns shown in Fig. 3 and 4 were measured after cooling down the samples.

In the case of the NaCl mixture the decomposition products were identified after the second (290 °C) and fourth step (400 °C). In accordance with the dehydrogenation pathway reported in the literature (reactions (1)–(4)),[16–18] reflections of CaH_2 and Al were found after decomposing the mixture at 290 °C. The $CaAl_2$ phase, formed at 400 °C, also coincides with the established dehydrogenation reactions.

In contrast to $Ca(AlH_4)_2$ + 2NaCl, the decomposition of the LiCl mixture appears to be more complex. Considering the TG-DSC measurements, especially the proceeding of the second step which consists of two sub-steps is of interest. Accordingly $Ca(AlH_4)_2$ + 2LiCl was decomposed at 260 °C (sub-step 1 of the second step, DSC effect L2.1) and at 290 °C (sub-step 2 of the second step, DSC effect L2.2). Unfortunately, the corresponding diffractograms do not allow a clear understanding of the respective dehydrogenation reactions due to their similarity.

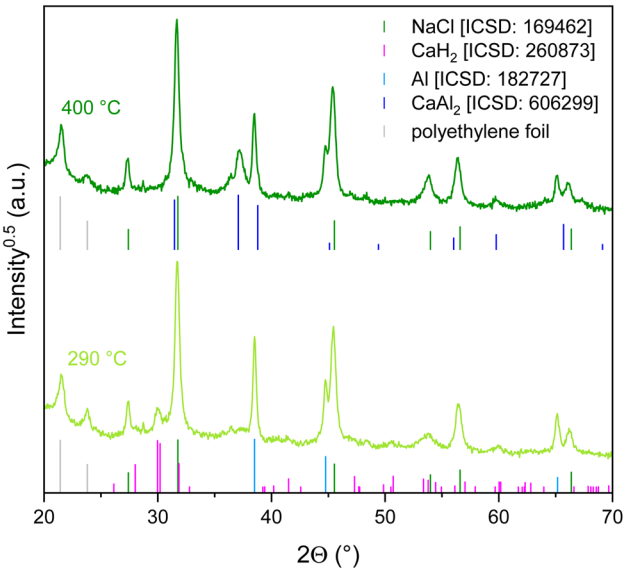

Fig. 3 X-ray powder diffraction patterns of the decomposition products of $Ca(AlH_4)_2$ + 2NaCl.

While Al can clearly be detected, the identification of the present hydride phase(s) is difficult due to overlapping reflections. The mixture heated to 260 °C most likely still contains $CaAlH_5$. This assignment seems sensible since the TG measurement shows that $CaAlH_5$ is not yet fully decomposed at 260 °C. Additionally, both dehydrogenation products probably contain CaH_2 and CaHCl. Analogously to $Sr(AlH_4)_2$ + 2LiCl,[10] the CaHCl phase is probably formed from CaH_2 and LiCl eqn (11).

$$CaH_2 + LiCl \rightarrow CaHCl + LiH \quad (11)$$

Like the $Ca(AlH_4)_2$ + 2NaCl mixture, $Ca(AlH_4)_2$ + 2LiCl decomposes to $CaAl_2$ in the fourth step.

To further investigate the second dehydrogenation step of the LiCl mixture, the decomposition of $Ca(AlH_4)_2$ + 2LiCl was also followed *in situ* by means of X-ray diffraction. The collected diffractograms are shown in Fig. 5.

Table 1 Onset temperatures (T_{Onset}) of the $Ca(AlH_4)_2$ decomposition reactions in comparison to literature values. The onset temperatures of this study were determined using DSC measurements at heating rates of 5 K min^{-1}

Mixture		1st step	2nd step	3rd step
$Ca(AlH_4)_2$ + 2NaCl	DSC effect	N1	N2	N3
	T_{Onset} (°C)	156 ± 9	250 ± 5	311 ± 2
$Ca(AlH_4)_2$ + 2LiCl	DSC effect	L1	L2.1	L3
	T_{Onset} (°C)	167 ± 4	235 ± 5	319 ± 3
Literature	T_{Onset} (°C)	80 (ref. 18)–180 (ref. 35)	180 (ref. 18)–250 (ref. 16)	350–360 (ref. 18)

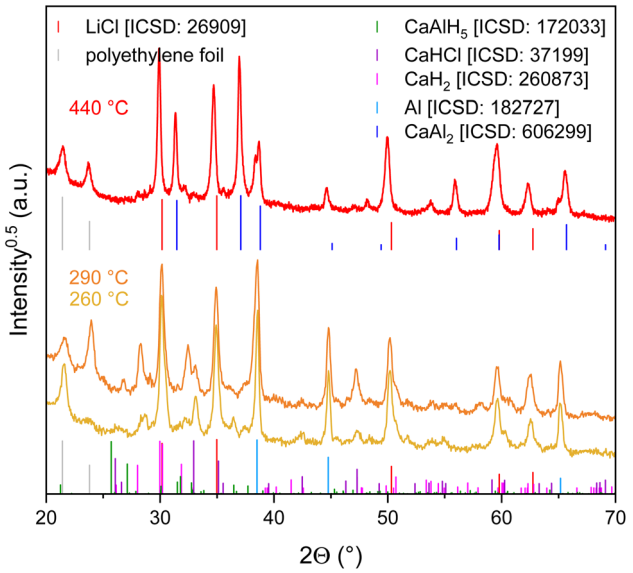

Fig. 4 X-ray powder diffraction patterns of the decomposition products of $Ca(AlH_4)_2$ + 2LiCl.

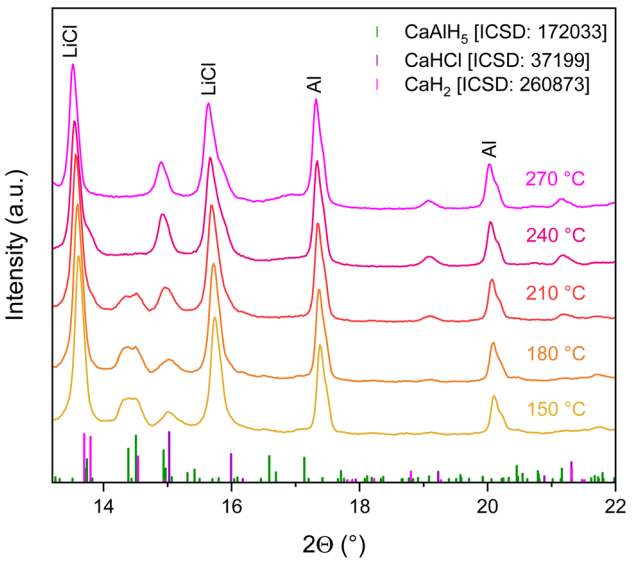

Fig. 5 *In situ* X-ray powder diffraction patterns of the $Ca(AlH_4)_2$ + 2LiCl dehydrogenation.

According to these, the decomposition of $CaAlH_5$ appears to be completed at 240 °C under the measuring conditions, as its reflections can no longer be observed at this temperature. Shoulders, which can be assigned to the formation of CaH_2 and CaHCl, respectively, emerge on the LiCl reflections at 13.6° and 15.7° with the onset of the $CaAlH_5$ dehydrogenation at 210 °C. Moreover, the intensity of the signal at 15° increases, also indicating the formation of CaHCl. Since the reflections of CaH_2 and CaHCl appear at the same temperature, it seems that both hydrides are formed simultaneously from $CaAlH_5$. Hence, these *in situ* measurements do not allow a significantly deeper understanding of the decomposition pathway of $Ca(AlH_4)_2$ + 2LiCl. However, the decomposition of $CaAlH_5$ to Al is confirmed once more by the observed increase of the Al reflection intensities during the *in situ* decomposition experiment.

3.3 Determination of the apparent activation energy of the $Ca(AlH_4)_2$ and $CaAlH_5$ dehydrogenation

In order to verify that the shift in the onset temperatures of the dehydrogenation reactions of the different mixtures is not due to varying decomposition kinetics, the apparent activation energies (E_a) of the respective reactions were determined using Kissinger plots. This method is based on eqn (12),[36] where β is the heating rate and T_P denotes the peak temperature.

$$\ln\left(\frac{\beta}{T_P^2}\,\mathrm{min\ K}\right) = -\frac{E_a}{RT_P} + A \qquad (12)$$

The Kissinger plots shown in Fig. 6 were derived from the peak temperatures obtained from DSC measurements at different heating rates (2 K min^{-1}, 5 K min^{-1}, 8 K min^{-1}, and 10 K min^{-1}). Two measurements were performed at each heating rate. The exothermic peak was used for the Kissinger plot of the 1st dehydrogenation event.

In the case of $Ca(AlH_4)_2$ + 2NaCl, the quality of the measurements made at heating rates of 2 K min^{-1} did not allow the determination of the peak temperature of the first step. Therefore, only the other ones, performed at higher heating rates, were used to generate the corresponding Kissinger plot. Moreover, due to the deviating peak temperatures for the $Ca(AlH_4)_2$ decomposition of the NaCl mixture, two different fits were necessary to obtain the apparent activation energy of its dehydrogenation. However, the determined values are in good agreement, so only their mean value is given in Table 2. The obtained apparent activation energies for the decomposition reactions of $Ca(AlH_4)_2$ + 2LiCl and $Ca(AlH_4)_2$ + 2NaCl are summarised in Table 2.

The results confirm that the first decomposition step is not influenced by the by-product as the respective values are in good agreement. Furthermore, the determined activation energies show that the different milling times do not affect the dehydrogenation kinetics significantly. Therefore, a comparison between the two mixtures is legitimate.

In contrast to the first decomposition step, the values obtained for the second one deviate from each other. Although $CaAlH_5$ + 2LiCl dehydrogenates at lower temperatures than the NaCl mixture (see Table 1), the opposite trend can be observed for the apparent activation energies. Thus, it appears likely that those correspond to different reactions which further supports the previously stated influence of the halides on the dehydrogenation pathway of $CaAlH_5$.

The comparison of the determined activation energies with literature values shows significant differences between those obtained for the first step. The ones determined for the second step lie in the same range. Since apparent activation energies are generally strongly dependent on the synthesis procedure, differences in these are probably the cause of the observed deviations.

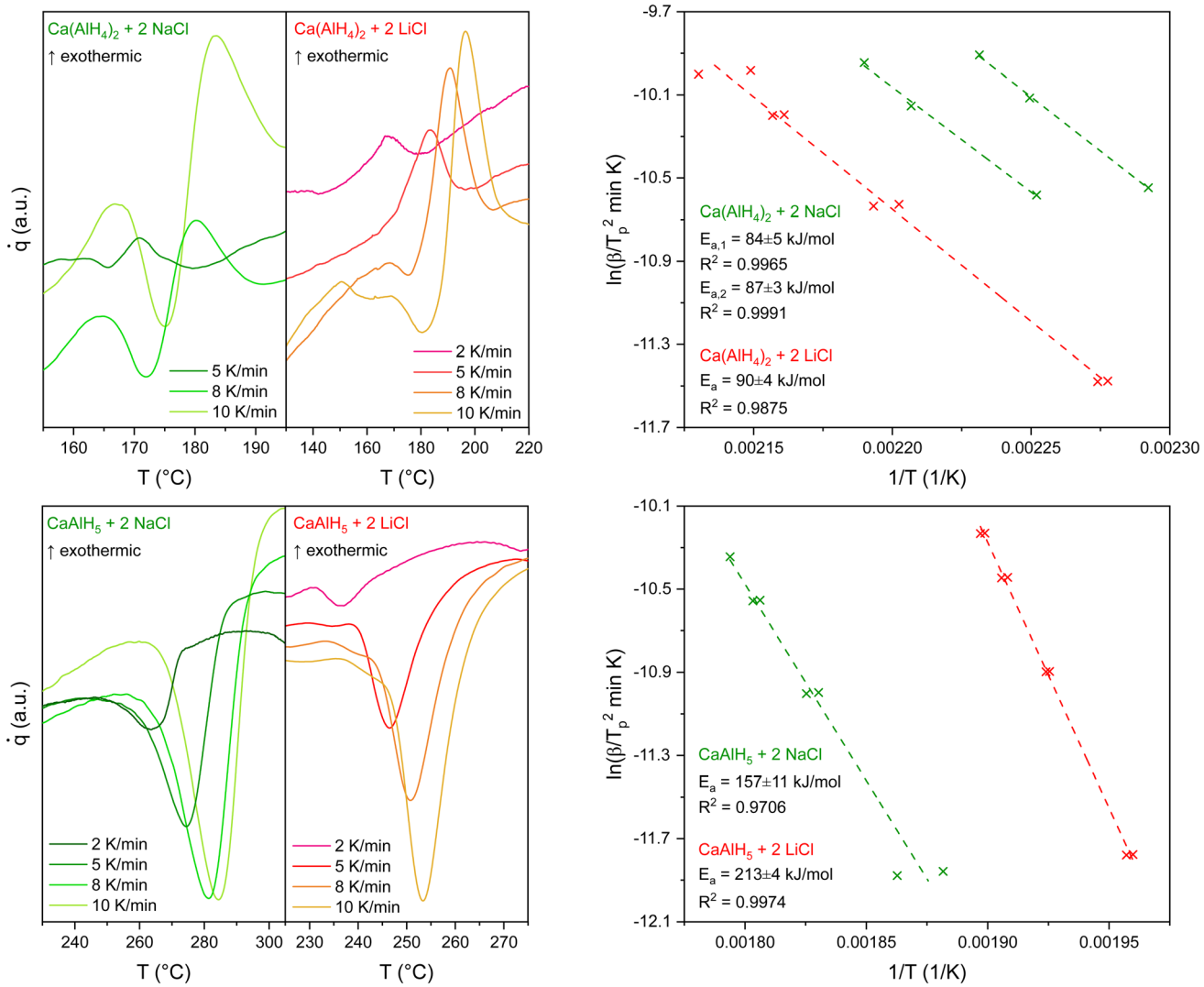

Fig. 6 DSC measurements and Kissinger plots for the first (above) and second (beneath) decomposition step of $Ca(AlH_4)_2$ + 2MCl (M = Li, Na).

Table 2 Apparent activation energies of the first and second step of the decomposition of $Ca(AlH_4)_2$ + 2MCl (M = Li, Na) in comparison to literature data

		$Ca(AlH_4)_2$ + 2NaCl	$Ca(AlH_4)_2$ + 2LiCl
1st step	This study	86 ± 5 kJ mol^{-1}	90 ± 4 kJ mol^{-1}
	Literature	62.8 kJ mol^{-1} (ref. 37)	135 kJ mol^{-1} (ref. 33)
2nd step	This study	157 ± 11 kJ mol^{-1}	213 ± 4 kJ mol^{-1}
	Literature	154.9 kJ mol^{-1} (ref. 37)	183 kJ mol^{-1} (ref. 33)
		153.4 kJ mol^{-1} (ref. 17)	

3.4 Heat capacity and absolute entropy of $Ca(AlH_4)_2$ and $CaAlH_5$

3.4.1 $Ca(AlH_4)_2$. Using calorimetric measurements of both $Ca(AlH_4)_2$ + 2MCl (M = Li, Na) mixtures, the heat capacity function in the temperature range from 2 K to 360 K and the absolute entropy at 298.15 K of the alanate were obtained. In order to derive the heat capacity of $Ca(AlH_4)_2$ from that of the mixture an additive composition of the heat capacity of the mixture according to eqn (13) was assumed. Further assuming a sample composition of $Ca(AlH_4)_2$: MCl of 1 : 2 and using literature heat capacity data for LiCl (0–20 K,[38] 20–300 K,[39] and 300–360 K (ref. 40)) and NaCl,[10] the heat capacity of the alanate was obtained from that of the mixture. The determined values are depicted in Fig. 7.

$$C_p^{sample} = x^{Ca(AlH_4)_2} C_p^{Ca(AlH_4)_2} + x^{MCl} C_p^{MCl} \quad (13)$$

Although this method was already verified in our studies on $Mg(AlH_4)_2$ (ref. 9) and $Sr(AlH_4)_2$,[10] its applicability to $Ca(AlH_4)_2$ was checked nevertheless. For this means, the heat capacities of the alanate were calculated from the measurements of both mixtures in the temperature range from 283 K to 360 K. Since the obtained values agree well with each other (see Fig. 7), the applied method is also suitable to determine the heat capacity function of $Ca(AlH_4)_2$ from that of $Ca(AlH_4)_2$ + 2MCl (M = Li, Na). Additionally, the good agreement of the values indicates

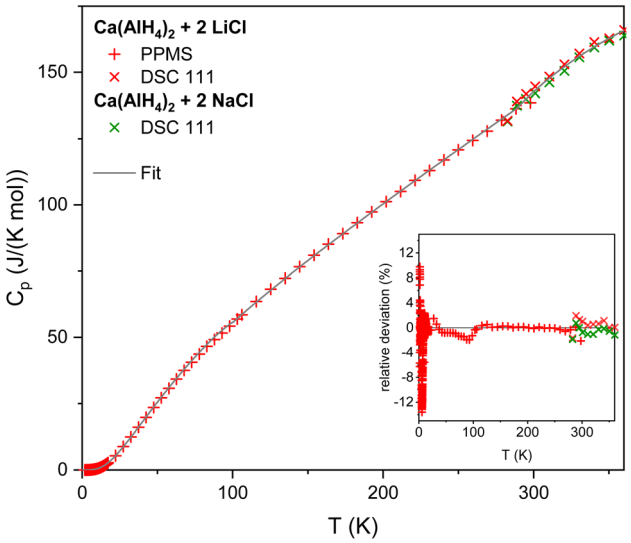

Fig. 7 Temperature dependency of the molar heat capacity of $Ca(AlH_4)_2$ derived from that of the mixtures. The relative deviation of the experimental values from the fitted curve is shown in the insert.

that the heat capacity of $Ca(AlH_4)_2$ is not affected by the halides NaCl and LiCl.

The measured heat capacities show no indication of the occurrence of phase transitions of $Ca(AlH_4)_2$ in the investigated temperature range. After dividing this range in four appropriate intervals, the respective data were fitted using established polynomial functions (eqn (14)–(17)) to obtain the heat capacity of $Ca(AlH_4)_2$ as a function of the temperature. The respective fit functions are stated in the following and the determined coefficients are listed in Table 3.

$$0-5\ \mathrm{K}: C_\mathrm{p}\Big/\mathrm{J(K\ mol)^{-1}} = b\frac{T}{K} + d\frac{T^3}{K^3} \quad (14)$$

$$5-100\ \mathrm{K}: C_\mathrm{p}\Big/\mathrm{J(K\ mol)^{-1}} = a + b\frac{T}{K} + c\frac{T^2}{K^2} + d\frac{T^3}{K^3} + e\frac{T^4}{K^4} + f\frac{T^5}{K^5} + g\frac{T^7}{K^7} + h\frac{K^2}{T^2} + i\frac{K}{T} \quad (15)$$

$$100-290\ \mathrm{K}: C_\mathrm{p}\Big/\mathrm{J(K\ mol)^{-1}} = a + b\frac{T}{K} + c\frac{T^2}{K^2} + h\frac{K^2}{T^2} \quad (16)$$

$$290-360\ \mathrm{K}: C_\mathrm{p}\Big/\mathrm{J(K\ mol)^{-1}} = a + b\frac{T}{K} + c\frac{T^2}{K^2} + h\frac{K^2}{T^2} \quad (17)$$

In Fig. 7 the fitted functions are compared to the measured data. The relative deviation of the experimental values from the fit, which is ±14% below 20 K and ±2% above 20 K, is shown in the insert of the same graph.

The absolute entropy of $Ca(AlH_4)_2$ at 298.15 K was calculated to be 141.3 ± 3.0 J $(K\ mol)^{-1}$ from the herein reported heat capacity functions using eqn (18).

$$S(298.15\ \mathrm{K}) = \int_0^{298.15\ \mathrm{K}} \frac{C_\mathrm{p}}{T}\mathrm{d}T \quad (18)$$

3.4.2 $CaAlH_5$. While the heat capacity and absolute entropy of $Ca(AlH_4)_2$ were determined calorimetrically, the respective values for $CaAlH_5$ were obtained using the quasi-harmonic approximation, which gives the Gibbs energy of a solid as a function of temperature and pressure. The computations were performed as described in ref. 10 based on the initial crystal structure of $CaAlH_5$ reported in ref. 41. By evaluating the negative of the first temperature derivative of the Gibbs energy at 298.15 K, the absolute entropy of $CaAlH_5$ at this temperature was obtained as 78.0 J $(K\ mol)^{-1}$. The isobaric heat capacity was calculated by multiplying the second temperature derivative of the Gibbs energy with the temperature. In this way, the heat capacity was evaluated for temperatures up to and including 530 K (see Fig. 8).

To validate the DFT computed heat capacity values, the modified Neumann–Kopp rule, which allows to estimate the heat capacities of complex compounds from the heat capacities of their simple constituents,[43] was used. The suitability of the modified Neumann–Kopp rule for estimating the heat capacities of complex aluminium hydrides was already established by us in ref. 10. Consequently, no general review of this approach is provided in this study.

According to the modified Neumann–Kopp rule, the heat capacity of $CaAlH_5$ can be described by the sum of those of CaH_2

Table 3 Coefficients of the fitted heat capacity functions of $Ca(AlH_4)_2$

T interval (K)	0–5	5–100	100–290	290–360
a		7.43414	1.69018×10^{1}	3.47691×10^{2}
b	6.56561×10^{-4}	−1.02199	4.38790×10^{-1}	-4.96854×10^{-1}
c		6.57500×10^{-2}	-7.99252×10^{-5}	5.34273×10^{-4}
d	4.36985×10^{-4}	-1.21000×10^{-3}		
e		1.13315×10^{-5}		
f		-4.66147×10^{-8}		
g		3.62645×10^{-13}		
h		3.13462×10^{1}	-4.38967×10^{4}	-9.36430×10^{6}
i		-2.50748×10^{1}		
R^2	0.9997	1.0000	0.9995	0.9813
FitStdErr	0.00026	0.01403	0.00822	1.52100

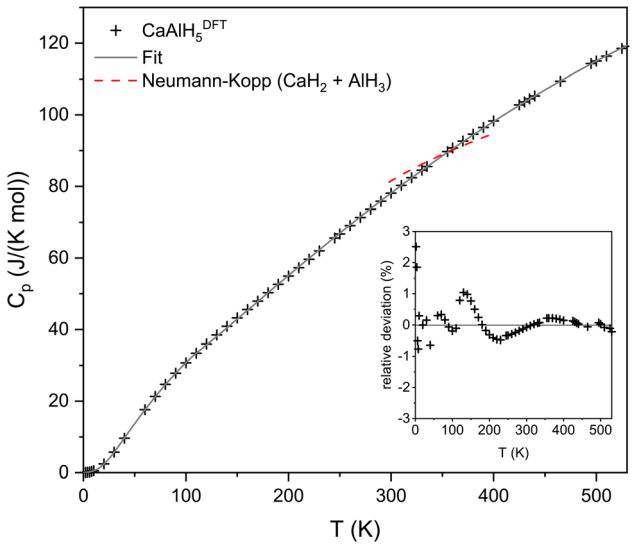

Fig. 8 Temperature dependency of the molar heat capacity of $CaAlH_5$ in comparison to values approximated by the modified Neumann–Kopp rule. The data for the approximation were taken from ref. 42. The relative deviation of the experimental values from the fitted curve is shown in the insert.

and AlH_3. The required literature data were taken from the HSC database.[42] Since no data are available below 298 K and above 500 K for CaH_2 and AlH_3, respectively, the validation of the computed heat capacity data is only possible in the temperature range between 298 K and 500 K. However, as AlH_3 is reported to decompose at 398–473 K,[44] the Neumann–Kopp rule was only applied up to a temperature of 398 K. As can be seen from the comparison of the approximated and DFT values depicted in Fig. 8, both methods are generally in good agreement with each other. Therefore, we consider the DFT calculated heat capacities to be realistic.

In order to obtain the heat capacity of $CaAlH_5$ as a function of the temperature, the calculated values were fitted using polynomial functions as described previously for $Ca(AlH_4)_2$. The used fit functions can be found in the following and the determined coefficients are summarised in Table 4. A comparison of the fitted functions with the original data as well as the relative deviation between them, which is less than ±3% over the whole temperature range, are shown in Fig. 8.

$$4-20\ \mathrm{K}: C_\mathrm{p}\Big/\mathrm{J(K\ mol)^{-1}} = b\frac{T}{K} + d\frac{T^3}{K^3} + e\frac{T^5}{K^5} \qquad (19)$$

Table 4 Coefficients of the fitted heat capacity functions of $CaAlH_5$

T interval (K)	4–20	20–110	110–530
a		−10.52682	−2.83845
b	2.71600×10^{-2}	5.41020×10^{-1}	3.18030×10^{-1}
c		-1.29000×10^{-3}	-1.65435×10^{-4}
d	2.70327×10^{-4}		
e	-8.13679×10^{-8}		
f		1.06475×10^{3}	3.99282×10^{4}
R^2	1.0000	1.0000	0.9999
FitStdErr	2.15×10^{-3}	0.06768	0.21586

$$20-110\ \mathrm{K}: C_\mathrm{p}\Big/\mathrm{J(K\ mol)^{-1}} = a + b\frac{T}{K} + c\frac{T^2}{K^2} + f\frac{K^2}{T^2} \qquad (20)$$

$$110-530\ \mathrm{K}: C_\mathrm{p}\Big/\mathrm{J(K\ mol)^{-1}} = a + b\frac{T}{K} + c\frac{T^2}{K^2} + f\frac{K^2}{T^2} \qquad (21)$$

3.5 Thermodynamic evaluation of the influence of LiCl and NaCl on the thermal dehydrogenation of $CaAlH_5$

As both the XRD and kinetic investigations did not provide a full understanding of the influence of the halides on the dehydrogenation of $CaAlH_5$, we performed thermodynamic calculations to gain a deeper insight into their effect. For this purpose, the literature value in ref. 35 for the enthalpy of formation of $CaAlH_5$, which was calculated for 0 K using DFT, was extrapolated to 298.15 K applying Kirchhoff's law (eqn (22)).

$$\Delta_\mathrm{F}H(298.15\ \mathrm{K}) = \Delta_\mathrm{F}H(0\ \mathrm{K}) + \int_{0\ \mathrm{K}}^{298.15\ \mathrm{K}} \Delta_\mathrm{F}C_\mathrm{p}\mathrm{d}T \qquad (22)$$

The needed heat capacity data for Ca, Al, and H_2 were taken from the references listed in Table 5. If only heat capacity values were reported, those were fitted using eqn (23). The parameters of these fits are stated in Table 5. For $CaAlH_5$ the heat capacity function reported in this study was used. An enthalpy of formation of −240 kJ mol^{-1} was obtained. It has to be noted, that no reliable heat capacity data are available for H_2 below 50 K. However, we consider the resulting uncertainty of the extrapolated enthalpy value to be small due to the small contribution of $\int_{0\ \mathrm{K}}^{T} C_\mathrm{p}\mathrm{d}T$ at low temperatures.

$$C_\mathrm{p}\Big/\mathrm{J(K\ mol)^{-1}} = a + b\times10^{-3}\frac{T}{K} + c\times10^{5}\frac{K^2}{T^2} + d\times10^{-6}\frac{T^2}{K^2} \qquad (23)$$

In the thermodynamic assessment of the effect of LiCl and NaCl on the dehydrogenation of $CaAlH_5$ CaH_2, CaHCl, and Al, which were detected in the XRD measurements, were considered as possible decomposition products. Furthermore, presuming a similar behaviour of $CaAlH_5$ and $SrAlH_5$ we assume the formation of CaHCl eqn (24) to proceed analogously to that of SrHCl.[10]

$$\mathrm{CaAlH_5 + MCl \rightarrow CaHCl + Al + MH + \frac{3}{2}H_2 (M = Li,\ Na)} \qquad (24)$$

In order to evaluate the influence of the two halides, the Gibbs free reaction energies for the possible decomposition reactions were calculated as a function of the temperature using the thermodynamic data listed in Tables 5 and 6. Their temperature dependence is shown in Fig. 9 and 10.

In accordance with the previous investigations, it can be seen in Fig. 9 that NaCl does not affect the dehydrogenation of $CaAlH_5$ as its decomposition to CaH_2, Al, and H_2 is thermodynamically most likely.

In contrast, when the mixture contains LiCl both the formation of CaHCl and CaH_2 are feasible from

Table 5 Heat capacity data used in this study, the abbreviations NK and Fit are assigned to data approximated by the Neumann–Kopp rule and data fitted by us, respectively. The coefficients describe the heat capacity according to the following function: $C_p/\mathrm{J(K\ mol)^{-1}} = a + b \times 10^{-3}\frac{T}{K} + c \times 10^{5}\frac{K^2}{T^2} + d \times 10^{-6}\frac{T^2}{K^2} + e \times 10^{6}\frac{K^3}{T^3}$

Compound	T_1 (K)	T_2 (K)	a	b	c	d	e	Ref.
Al^{Fit}	15	80	−1.180	42.456	0	1133.179	0	45
	80	350	21.18	24.45	−1.791	−30.17	7.654	46
	298.15	933	32.974	−20.677	−4.138	23.753	0	42
AlH_3	298.15	500	49.387	24.072	−14.588	0.637	0	42
Ca^{Fit}	5	45	−0.695	51.370	0	4064.848	0	47
Fit	50	150	10.220	163.293	−0.136	−485.063	0	47
Fit	150	300	25.535	−0.980	−0.561	12.903	0	47
$CaAl_2^{NK}$	298.15	716	82.259	−19.136	−5.603	47.499	0	42
$CaAl_4^{NK}$	298.15	716	148.207	−60.49	−13.879	95.005	0	42
CaH_2	298.15	1053	29.928	37.133	0	0	0	42
CaHCl	308	748	57.806	16.42	−10.06	0	0	48
H_2	50	298.15	22.496	17.044	0.365	11.122	0	42
	298.15	5000	25.855	4.837	1.584	−0.372	0	42
LiCl	298.15	883	44.707	17.924	−1.946	1.865	0	42
LiH	298.15	965	21.006	43.713	−4.525	0.01	0	42
NaCl	298.15	900	56.297	−13.015	−3.423	21.862	0	42
NaH	298.15	911	31.401	35.326	−4.92	0.008	0	42

a thermodynamic point of view as the corresponding Gibbs free energies are very similar in the temperature region of the $CaAlH_5$ + 2LiCl dehydrogenation (see Fig. 9). Thus, the sub-steps of the second dehydrogenation event in the TG-DSC measurements could be the result of the parallel formation of the two hydrides.

Furthermore, we found the apparent activation energies for the decomposition of $CaAlH_5$ + 2LiCl and $CaAlH_5$ + 2NaCl to differ significantly. Therefore, it seems likely that they belong to two different reactions. Since the dehydrogenation of $CaAlH_5$ + 2NaCl to CaH_2 occurs at higher temperatures than the decomposition of the LiCl mixture and since the thermodynamic driving force for the formation of CaHCl is initially slightly higher, we believe that the first sub-step belongs to the dehydrogenation of $CaAlH_5$ to CaHCl and the second one to the formation of CaH_2.

The thermodynamic calculations depicted in Fig. 10 show that the decomposition of the hydrides CaH_2 and CaHCl to first $CaAl_4$ and then to $CaAl_2$ occurs at similar temperatures, respectively. This result agrees with the dehydrogenation behaviour observed in the TG-DSC measurements. It has to be noted, that the enthalpies of formation of $CaAl_4$ and $CaAl_2$ used in the computations were determined by optimising the literature values[49] considering their formation temperatures.

Furthermore, the calculations support the notion that NaCl does not alter the decomposition pathway of $CaAlH_5$ as the formation of CaHCl from CaH_2 and NaCl is thermodynamically not feasible in the investigated temperature range.

In conclusion, $CaAlH_5$ + 2NaCl dehydrogenates according to the reactions (25)–(27). Thus, the DSC effects N2, N3, and N4 result from eqn (25)–(27), respectively.

$$CaAlH_5 \rightarrow CaH_2 + Al + \frac{3}{2}H_2 \quad (25)$$

$$\frac{1}{2}CaH_2 + 2Al \rightarrow \frac{1}{2}CaAl_4 + \frac{1}{2}H_2 \quad (26)$$

Table 6 Enthalpies of formation and absolute entropies used in this study. Values marked with Opt. were optimised based on literature data and formation temperatures, respectively

Compound	$\Delta_F H$ (298.15 K) (kJ mol^{-1})	S (298.15 K) (J (K mol)$^{-1}$)	Ref.
Al	0	28.280	42
$CaAl_2$	$-108.000^{Opt.}$	83.065	49
$CaAl_4$	$-121.000^{Opt.}$	127.238	49
$Ca(AlH_4)_2$	−247	141.3 ± 3.0	50, 51 and this study
$CaAlH_5$	−240	78.0	52 and this study
CaH_2	−181.558	41.401	42 and 53
CaHCl	−504.172	71.8	53 and 54
H_2	0	130.700	42
LiCl	−408.270	59.300	42
LiH	−90.542	20.041	42
NaCl	−411.120	72.132	42
NaH	−56.379	39.999	42

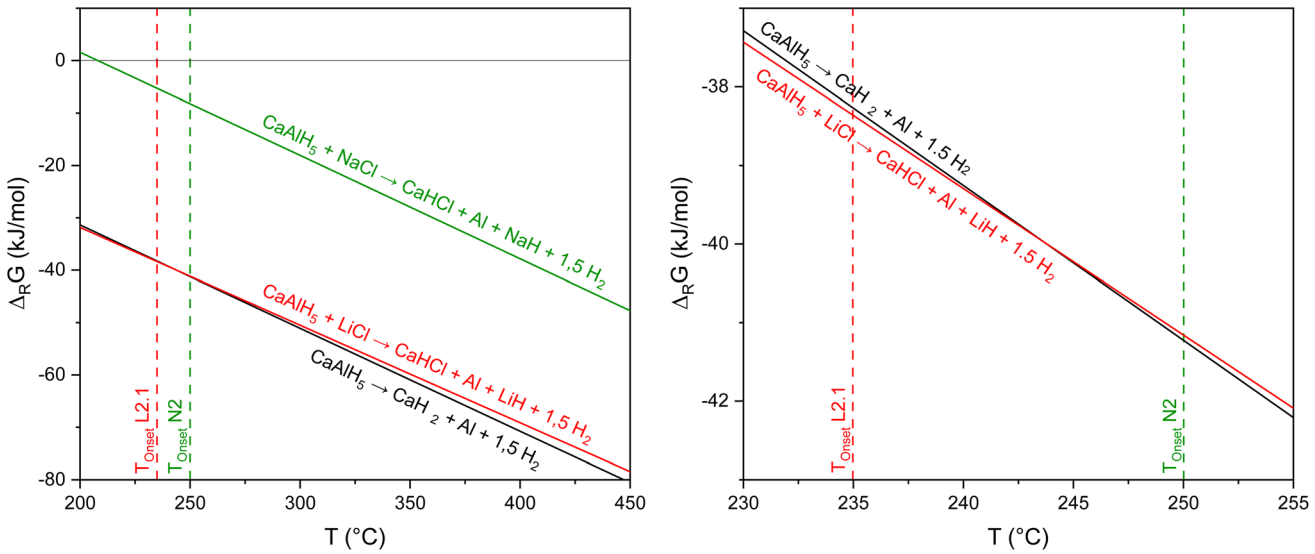

Fig. 9 Thermodynamic assessment of the decomposition of $CaAlH_5$ + 2MCl (M = Li, Na). The coloured dotted lines represent the onset temperatures of the second decomposition step of $Ca(AlH_4)_2$ + 2MCl. The right figure was created to allow a differentiation of the lines overlapping in the figure on the left.

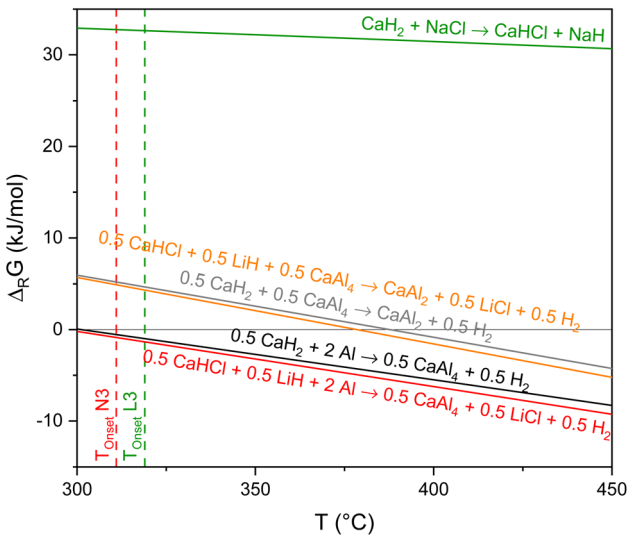

Fig. 10 Thermodynamic assessment of the decomposition of CaHX (X = H, Cl). The coloured dotted lines represent the onset temperatures of the third decomposition step of $Ca(AlH_4)_2$ + 2MCl.

$$\frac{1}{2}CaH_2 + \frac{1}{2}CaAl_4 \rightarrow CaAl_2 + \frac{1}{2}H_2 \quad (27)$$

In contrast, in the presence of LiCl, CaHCl is formed in addition to CaH_2. In this case the DSC effects L2.1 and L2.2 may be assigned to eqn (28) and (29), respectively. The effects L3 and L4 then correspond to eqn (30) and (31).

$$xCaAlH_5 + xLiCl \rightarrow xCaHCl + xAl + xLiH + \frac{3}{2}xH_2 (0 < x < 1) \quad (28)$$

$$(1-x)CaAlH_5 \rightarrow (1-x)CaH_2 + (1-x)Al + \frac{3}{2}(1-x)H_2 (0 < x < 1) \quad (29)$$

$$\frac{1}{2}CaHX + 2Al + \frac{1}{2}LiY \rightarrow \frac{1}{2}CaAl_4 + \frac{1}{2}LiCl + \frac{1}{2}H_2 (X = H,\ Y = Cl \text{ or } X = Cl,\ Y = H) \quad (30)$$

$$\frac{1}{2}CaHX + \frac{1}{2}CaAl_4 + \frac{1}{2}LiY \rightarrow CaAl_2 + \frac{1}{2}LiCl + \frac{1}{2}H_2 (X = H,\ Y = Cl \text{ or } X = Cl,\ Y = H) \quad (31)$$

As in the case of $Sr(AlH_4)_2$, the different effects of LiCl and NaCl on the decomposition behaviour of $CaAlH_5$ are probably the result of the differing thermodynamic stabilities of LiH ($\Delta_F H°$ (298.15 K) = −90.5 kJ mol^{-1} (ref. 42)) and NaH ($\Delta_F H°$ (298.15 K) = −56.4 kJ mol^{-1} (ref. 42)).[10] Due to the high stability of LiH, its formation is thermodynamically favoured. As a consequence, LiCl alters the dehydrogenation pathway of $CaAlH_5$.

3.6 Thermodynamic assessment of the potential of $Ca(AlH_4)_2$ and $CaAlH_5$ for reversible hydrogen storage applications

Using the determined thermodynamic data as well as the literature data in Tables 5 and 6, the ability of $Ca(AlH_4)_2$ and $CaAlH_5$ to reversibly store hydrogen was evaluated from a thermodynamic point of view by computing their respective dehydrogenation pressures in dependence of the temperature (Fig. 11). For this purpose, the literature values for the enthalpy of formation of $Ca(AlH_4)_2$,[50,51] which were calculated for 0 K using DFT, were

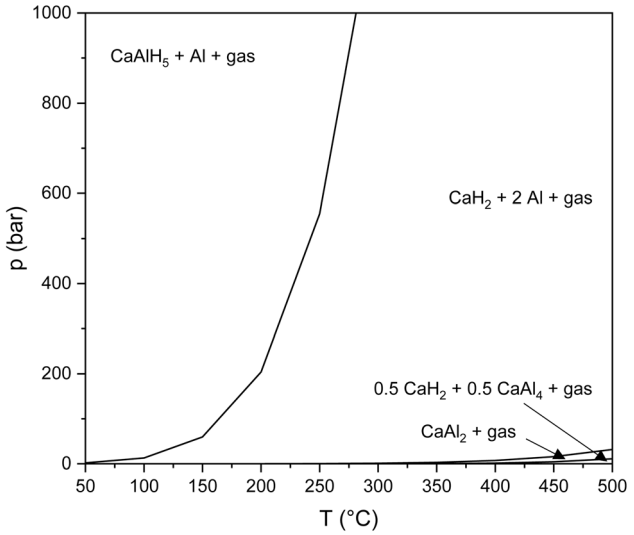

Fig. 11 Temperature dependency of the hydrogen pressure of the decomposition of $Ca(AlH_4)_2$.

extrapolated to 298.15 K as described previously for $CaAlH_5$. We obtained values of −235 kJ mol^{-1} and −258.3 kJ mol^{-1}. The presented calculations were made using the mean value of the enthalpies of formation obtained, which is −247 kJ mol^{-1}.

$Ca(AlH_4)_2$ can be considered unsuitable for reversible hydrogen storage applications due to its high hydrogenation pressure. In contrast, the hydrogenation of CaH_2 and Al to $CaAlH_5$ at a pressure of 200 bar is thermodynamically possible up to 200 °C.

Since we were not able to fully clarify the decomposition pathway of $CaAlH_5$ in the presence of LiCl, its hydrogenation behaviour could not be assessed thermodynamically.

4 Conclusions

Within this study we investigated the influence of the by-products LiCl and NaCl on the thermal decomposition of $Ca(AlH_4)_2$ by means of X-ray diffraction, the Kissinger method and thermodynamic computations. While we found no effect of the halides on the dehydrogenation of the alanate itself, the decomposition of its dehydrogenation product $CaAlH_5$ depends on the halides. No change of the dehydrogenation pathway occurs in the presence of NaCl. In contrast, the second decomposition step splits into two sub-steps when the mixture contains LiCl. Additionally, CaHCl is formed in this step alongside the normally produced CaH_2.

Besides the study of the thermal dehydrogenation of $Ca(AlH_4)_2$, the alanate and $CaAlH_5$ were characterised thermodynamically. The heat capacity function in the temperature range from 2 K to 360 K and the absolute entropy of $Ca(AlH_4)_2$ were determined by means of calorimetry. DFT calculations were used to obtain the heat capacity function (4–530 K) and the absolute entropy of $CaAlH_5$. The values for the absolute entropies of $Ca(AlH_4)_2$ and $CaAlH_5$ at 298.15 K are 141.3 ± 3.0 J (K mol)$^{-1}$ and 78.0 J (K mol)$^{-1}$, respectively. The enthalpies of formation of $Ca(AlH_4)_2$ and $CaAlH_5$ were calculated to be −247 kJ mol^{-1} and −240 kJ mol^{-1}, respectively.

Finally, the hydrogenation behaviour of the complex hydrides was evaluated thermodynamically. While $Ca(AlH_4)_2$ has to be considered unsuited for reversible hydrogen storage applications, reversible hydrogen storage may be achieved in the $CaAlH_5$ system at 200 °C and 200 bar.

Data availability

The data supporting this article have been included as part of the ESI.†

Author contributions

Franziska Habermann: investigation, visualization, writing – original draft. Anneliese Wirth: investigation, writing – review & editing. Konrad Burkmann: validation, writing – review & editing. Jakob Kraus: investigation, writing – original draft. Bianca Störr: investigation. Hartmut Stöcker: investigation, writing – original draft. Jürgen Seidel: writing – review & editing. Jens Kortus: resources, writing – review & editing. Roman Gumeniuk: investigation, resources. Klaus Bohmhammel: investigation, writing – review & editing. Florian Mertens: funding acquisition, Resources, writing – review & editing.

Conflicts of interest

There are no conflicts to declare.

Acknowledgements

The reported research activities have been financially supported by the Deutsche Forschungsgemeinschaft (DFG, project number 449160425). The heat capacity measurements in this study were performed on the DynaCool-12 system acquired within the DFG project 422219901. We also thank the URZ in Freiberg for computational time and support. The computations at the URZ were performed on the computing cluster of the Faculty of Mathematics and Computer Science of the Technische Universität Bergakademie Freiberg; this cluster is funded by the DFG (project number 397252409). Additionally, we thank Dirk Meyer for providing the Bruker D8 Advance X-ray diffractometer for the *in situ* measurements at the Centre for Efficient High Temperature Processes and Materials Conversion.

References

1 M. Hirscher, V. A. Yartys, M. Baricco, J. Bellosta von Colbe, D. Blanchard, R. C. Bowman, D. P. Broom, C. E. Buckley, F. Chang, P. Chen, Y. W. Cho, J.-C. Crivello, F. Cuevas, W. I. David, P. E. de Jongh, R. V. Denys, M. Dornheim, M. Felderhoff, Y. Filinchuk, G. E. Froudakis, D. M. Grant, E. M. Gray, B. C. Hauback, T. He, T. D. Humphries, T. R. Jensen, S. Kim, Y. Kojima, M. Latroche, H.-W. Li, M. V. Lototskyy, J. W. Makepeace, K. T. Møller, L. Naheed,

P. Ngene, D. Noréus, M. M. Nygård, S.-I. Orimo, M. Paskevicius, L. Pasquini, D. B. Ravnsbæk, M. Veronica Sofianos, T. J. Udovic, T. Vegge, G. S. Walker, C. J. Webb, C. Weidenthaler and C. Zlotea, *J. Alloys Compd.*, 2020, **827**, 153548–153588.
2 Y. Liu, D. Chabane and O. Elkedim, *Energies*, 2021, **14**, 5758.
3 Z. Cao, F. Habermann, K. Burkmann, M. Felderhoff and F. Mertens, *Hydrogen*, 2024, **5**, 241–279.
4 J. J. Vajo, F. Mertens, C. C. Ahn, R. C. Bowman and B. Fultz, *J. Phys. Chem. B*, 2004, **108**, 13977–13983.
5 J. J. Vajo, S. L. Skeith and F. Mertens, *J. Phys. Chem. B*, 2005, **109**, 3719–3722.
6 J. Ortmeyer, A. Bodach, L. Sandig-Predzymirska, B. Zibrowius, F. Mertens and M. Felderhoff, *ChemPhysChem*, 2019, **20**, 1360–1368.
7 L. Sandig-Predzymirska, J. Ortmeyer, J. Wagler, E. Brendler, F. Habermann, M. Anders, M. Felderhoff and F. Mertens, *Dalton Trans.*, 2020, **49**, 17689–17698.
8 F. Habermann, K. Burkmann, B. Hansel, B. Störr, C. Schimpf, J. Seidel, M. Bertau and F. Mertens, *Dalton Trans.*, 2023, **52**, 4880–4890.
9 F. Habermann, A. Wirth, K. Burkmann, B. Störr, J. Seidel, R. Gumeniuk, K. Bohmhammel and F. Mertens, *ChemPhysChem*, 2024, **25**, e202300748–e202300759.
10 F. Habermann, K. Burkmann, J. Kraus, B. Störr, J. Seidel, J. Kortus, R. Gumeniuk, K. Bohmhammel and F. Mertens, *J. Alloys Compd.*, 2024, **980**, 173476–173488.
11 K. Burkmann, F. Habermann, E. Schumann, J. Kraus, B. Störr, H. Schmidt, E. Brendler, J. Seidel, K. Bohmhammel, J. Kortus and F. Mertens, *New J. Chem.*, 2024, **48**, 2743–2754.
12 B. Bogdanović and M. Schwickardi, *J. Alloys Compd.*, 1997, **253–254**, 1–9.
13 A. E. Finholt, G. D. Barbaras, G. K. Barbaras, G. Urry, T. Wartik and H. I. Schlesinger, *J. Inorg. Nucl. Chem.*, 1955, **1**, 317–325.
14 M. Fichtner, C. Frommen and O. Fuhr, *Inorg. Chem.*, 2005, **44**, 3479–3484.
15 H. Kabbour, C. C. Ahn, S.-J. Hwang, R. C. Bowman and J. Graetz, *J. Alloys Compd.*, 2007, **446–447**, 264–266.
16 M. Mamatha, B. Bogdanovic, M. Felderhoff, A. Pommerin, W. Schmidt, F. Schuth and C. Weidenthaler, *J. Alloys Compd.*, 2006, **407**, 78–86.
17 C. Li, X. Xiao, P. Ge, J. Xue, S. Li, H. Ge and L. Chen, *Int. J. Hydrogen Energy*, 2012, **37**, 936–941.
18 M. Mamatha, C. Weidenthaler, A. Pommerin, M. Felderhoff and F. Schüth, *J. Alloys Compd.*, 2006, **416**, 303–314.
19 *Crystallographic Databases*, ed. F. H. Allen, G. Bergerhoff and R. Sievers, International Union of Crystallography, Chester, 1987.
20 D. Thomas, M. Abdel-Hafiez, T. Gruber, R. Hüttl, J. Seidel, A. U. Wolter, B. Büchner, J. Kortus and F. Mertens, *J. Chem. Thermodyn.*, 2013, **64**, 205–225.
21 S. Loos, D. Gruner, M. Abdel-Hafiez, J. Seidel, R. Hüttl, A. U. Wolter, K. Bohmhammel and F. Mertens, *J. Chem. Thermodyn.*, 2015, **85**, 77–85.
22 Q. Shi, C. L. Snow, J. Boerio-Goates and B. F. Woodfield, *J. Chem. Thermodyn.*, 2010, **42**, 1107–1115.
23 G. K. White and S. J. Collocott, *J. Phys. Chem. Ref. Data*, 1984, **13**, 1251–1257.
24 G. Della Gatta, M. J. Richardson, S. M. Sarge and S. Stølen, *Pure Appl. Chem.*, 2006, **78**, 1455–1476.
25 P. Hohenberg and W. Kohn, *Phys. Rev.*, 1964, **136**, B864–B871.
26 W. Kohn and L. J. Sham, *Phys. Rev.*, 1965, **140**, A1133–A1138.
27 P. Giannozzi, S. Baroni, N. Bonini, M. Calandra, R. Car, C. Cavazzoni, D. Ceresoli, G. L. Chiarotti, M. Cococcioni, I. Dabo, A. Dal Corso, S. de Gironcoli, S. Fabris, G. Fratesi, R. Gebauer, U. Gerstmann, C. Gougoussis, A. Kokalj, M. Lazzeri, L. Martin-Samos, N. Marzari, F. Mauri, R. Mazzarello, S. Paolini, A. Pasquarello, L. Paulatto, C. Sbraccia, S. Scandolo, G. Sclauzero, A. P. Seitsonen, A. Smogunov, P. Umari and R. M. Wentzcovitch, *J. Phys.: Condens. Matter*, 2009, **21**, 395502–395521.
28 P. Giannozzi, O. Andreussi, T. Brumme, O. Bunau, M. Buongiorno Nardelli, M. Calandra, R. Car, C. Cavazzoni, D. Ceresoli, M. Cococcioni, N. Colonna, I. Carnimeo, A. Dal Corso, S. de Gironcoli, P. Delugas, R. A. DiStasio, A. Ferretti, A. Floris, G. Fratesi, G. Fugallo, R. Gebauer, U. Gerstmann, F. Giustino, T. Gorni, J. Jia, M. Kawamura, H.-Y. Ko, A. Kokalj, E. Küçükbenli, M. Lazzeri, M. Marsili, N. Marzari, F. Mauri, N. L. Nguyen, H.-V. Nguyen, A. Otero-de-la Roza, L. Paulatto, S. Poncé, D. Rocca, R. Sabatini, B. Santra, M. Schlipf, A. P. Seitsonen, A. Smogunov, I. Timrov, T. Thonhauser, P. Umari, N. Vast, X. Wu and S. Baroni, *J. Phys.: Condens. Matter*, 2017, **29**, 465901–465931.
29 P. Giannozzi, O. Baseggio, P. Bonfà, D. Brunato, R. Car, I. Carnimeo, C. Cavazzoni, S. de Gironcoli, P. Delugas, F. Ferrari Ruffino, A. Ferretti, N. Marzari, I. Timrov, A. Urru and S. Baroni, *J. Chem. Phys.*, 2020, **152**, 154105–154116.
30 P. E. Blöchl, *Phys. Rev. B: Condens. Matter Mater. Phys.*, 1994, **50**, 17953–17979.
31 A. Dal Corso, *Comput. Mater. Sci.*, 2014, **95**, 337–350.
32 J. P. Perdew, K. Burke and M. Ernzerhof, *Phys. Rev. Lett.*, 1996, **77**, 3865–3868.
33 R. Varin, E. Kościuczyk and T. Czujko, *Materials*, 2015, **8**, 3479–3490.
34 K. Suárez-Alcántara, J. R. Tena-Garcia and R. Guerrero-Ortiz, *Materials*, 2019, **12**, 2724–2787.
35 V. V. Gavrilenko, Y. N. Karaksin and L. I. Zakharkin, *Zh. Obshch. Khim.*, 1972, **42**, 1564–1569.
36 H. E. Kissinger, *Anal. Chem.*, 1957, **29**, 1702–1706.
37 X. Xiao, C. Li, L. Chen, X. Fan, H. Kou and Q. Wang, *J. Alloys Compd.*, 2011, **509S**, S743–S746.
38 D. F. Moyer, *J. Phys. Chem. Solids*, 1965, **26**, 1459–1462.
39 D. A. Shirley, *J. Am. Chem. Soc.*, 1960, **82**, 3841–3843.
40 M. W. Chase, *NIST-JANAF Thermochemical Tables*, American Institute of Physics, Woodbury, NY, 4th edn, 1998.
41 T. Sato, M. H. Sørby, K. Ikeda, S. Sato, B. C. Hauback and S. Orimo, *J. Alloys Compd.*, 2009, **487**, 472–478.
42 A. Roine, *HSC Chemistry*, 2021.

43 L. Qiu and M. A. White, *J. Chem. Educ.*, 2001, **78**, 1076–1079.
44 G. Sandrock, J. Reilly, J. Graetz, W.-M. Zhou, J. Johnson and J. Wegrzyn, *Appl. Phys. A*, 2005, **80**, 687–690.
45 W. F. Giauque and P. F. Meads, *J. Am. Chem. Soc.*, 1941, **63**, 1897–1901.
46 Y. Takahashi, T. Azumi and Y. Sekine, *Thermochim. Acta*, 1989, **139**, 133–137.
47 B. S. Hemingway and R. A. Robie, *J. Chem. Thermodyn.*, 1997, **29**, 211–220.
48 S. S. Kumar, S. Ghosh, M. Sahu and R. Ganesan, *J. Chem. Sci.*, 2019, **131**, 100–106.
49 D. Kevorkov, R. Schmid-Fetzer, A. Pisch, F. Hodaj and C. Colinet, *Int. J. Mater. Res.*, 2001, **92**, 953–958.
50 O. M. Løvvik and P. N. Molin, *AIP Conf. Proc.*, 2006, **837**, 85–90.
51 A. Klaveness, P. Vajeeston, P. Ravindran, H. Fjellvåg and A. Kjekshus, *Phys. Rev. B: Condens. Matter Mater. Phys.*, 2006, **73**, 094122–094128.
52 A. Klaveness, P. Vajeeston, P. Ravindran, H. Fjellvåg and A. Kjekshus, *J. Alloys Compd.*, 2007, **433**, 225–232.
53 P. Ehrlich, K. Peik and E. Koch, *Z. Anorg. Allg. Chem.*, 1963, **324**, 113–224.
54 K. Fiedler, dissertation, TU Bergakademie Freiberg, Freiberg, 2012.